Scientific Reports

https://doi.org/10.1038/s41598-026-39167-2

Article in Press

Macrophages recruited by implanted fibrin gels promote regeneration of injured lymphatic vessels

Received: 19 September 2025

Accepted: 3 February 2026

Published online: 20 March 2026

Cite this article as: Razavi M.S., Lei P., Amoozgar Z. *et al.* Macrophages recruited by implanted fibrin gels promote regeneration of injured lymphatic vessels. *Sci Rep* (2026). https://doi.org/10.1038/s41598-026-39167-2

Mohammad S. Razavi, Pin-Ji Lei, Zohreh Amoozgar, Meghan J. O'Melia, Kangsan Roh, Nichaluk Leartprapun, Seemantini K. Nadkarni, James W. Baish, Timothy P. Padera & Lance L. Munn

Macrophages recruited by implanted fibrin gels promote regeneration of injured lymphatic vessels

Mohammad S. Razavi[1#], Pin-Ji Lei[1], Zohreh Amoozgar[1†], Meghan J. O'Melia[1], Kangsan Roh[1], Nichaluk Leartprapun[2], Seemantini K. Nadkarni[2], James W. Baish[3], Timothy P. Padera[1*], Lance L. Munn[1*]

[1]Edwin L. Steele Laboratories, Department of Radiation Oncology, Massachusetts General Hospital Cancer Center, Massachusetts General Hospital and Harvard Medical School, Boston, MA 02114, USA

[2]Wellman Center for Photomedicine, Massachusetts General Hospital, Harvard Medical School, Boston, MA 02114 USA

[3]Biomedical Engineering, Bucknell University, Lewisburg, PA 17837, USA

* co-corresponding

#: Current Affiliation: Department of Mechanical and Materials Engineering, University of Nebraska-Lincoln, 900 N 16th St, Lincoln, NE 68588, United States of America

†: Current Affiliation: Sanofi, 270 Albany St., Cambridge, MA 02139, USA.

Correspondence to: lmunn@mgh.harvard.edu, tpadera@mgh.harvard.edu

Keywords: Lymphatic regeneration; Collecting lymphatic vessels; Lymphatic injury; Lymphatic pumping; Lymphedema

Abstract
Secondary lymphedema is a debilitating condition driven by impaired regeneration of lymphatic vasculature following lymphatic injury, surgical removal of lymph nodes in cancer patients, or infection. However, the extent to which collecting lymphatic vessels regenerate following injury remains unclear. Here, we employed a novel mouse model of lymphatic injury in combination with state-of-the-art lymphatic imaging to demonstrate that the implantation of an optimized fibrin gel following lymphatic vessel injury leads to the reconnection of the injured lymphatic vessel network through sprouting lymphangiogenesis of initial-like lymphatic vessels from the ends of the collecting lymphatic vessels, resulting in the restoration of lymph flow to the draining lymph node. Mechanistically, we found that fibrin implantation elevates the tissue levels of CCL5, a potent immune cell-recruiting chemokine. Notably, injured vessels in CCL5-KO mice made fewer connections following fibrin gel implantation. These novel findings shed light on the mechanisms underlying lymphatic regeneration and suggest that enhancing CCL5 signaling may be a promising therapeutic strategy for enhancing lymphatic regeneration.

One Sentence Summary: Implantation of fibrin gel promotes lymphatic regeneration after injury by elevating the chemokine CCL5 in tissue.

Introduction

The lymphatic system is key for tissue fluid homeostasis, immune surveillance, and lipid and macromolecule transport (1). The lymphatic system relies on the contractile activity of collecting lymphatic vessels to effectively transport lymph (2). Collecting lymphatic vessels have specialized lymphatic muscle cells (LMCs) that drive lymphatic contractions and intraluminal valves to ensure unidirectional lymph propulsion (2). Most lymphatic endothelial cells (LECs) arise embryonically from the cardinal vein, a process that is guided by lymphangiogenic factors such as VEGFC (3, 4). Such lymphangiogenic pathways are known to substantially decrease in adults, but can be reactivated in pathological scenarios, such as cancer and inflammation (5, 6).

The lymphatic vasculature is often damaged due to trauma, cancer surgery and therapy, and secondary to infection (7–9). Such lymphatic damage and subsequent pumping dysfunction lead to lymphedema, characterized by tissue swelling, chronic inflammation, fibrosis, and recurrent infections (10). Although lymphedema is prevalent among cancer survivors, therapeutic options are extremely limited, as there is no cure and no FDA-approved drugs for treating lymphedema. (10, 11). Some surgical interventions, such as lymphaticovenous anastomosis and vascularized lymph node transfer, have shown promise in preventing or reducing the volume of lymphedema (12–14). The underlying mechanisms that underpin these successes are being actively investigated (15, 16).

Recent research suggests that immune cells play a crucial role in lymphangiogenic responses and collateralization following injury (17, 18). Macrophages secrete factors known to be important in cancer and inflammation-associated lymphangiogenesis (19–22). More recently, CD4+ T lymphocytes have been proposed to inhibit the regeneration of lymphatic vessels by secreting anti-lymphangiogenic cytokines such as IFN-γ, TGFβ, IL-4, and IL-13 (23). The inhibition of lymphocyte infiltration following lymphatic damage has also led to improved lymphatic collateralization and lymphatic function in mice (23). Leukotriene B4 (LTB4), a mediator of inflammation that is elevated in lymphedema patients, has also been found to promote lymphatic sprouting at low doses while causing LEC damage and apoptosis at higher concentrations (24). In addition, cytokines such as TNF-α and IL-1α have been shown to recruit cells secreting lymphangiogenic factors (25–27). Strategies to promote lymphatic regeneration, such as gene and growth factor therapies, the application of natural and synthetic hydrogels, and engineered lymphatic vasculature, have also gained attention (28, 29). In mice, a combination of lymph node transplantation and VEGF-C therapy has been shown to repair damaged lymphatic vasculature after lymph node resection (30). The application of fibrillar collagen following node resection has also improved lymphatic density at the injury site (31). Seeding LECs with other cell types, such as fibroblasts or adipocyte-derived cells, in collagen hydrogels can also promote the growth of new lymphatic capillaries (32, 33).

Despite these efforts, the regeneration and repair of larger collecting lymphatic vessels remains elusive, and the mechanisms that drive these responses are largely unexplored. As it is one of the ultimate products of blood coagulation, fibrin plays a crucial role as the first scaffold that cells encounter after injury, facilitating the adhesion of various immune cells, including platelets, neutrophils, and macrophages, which in turn aid in tissue regeneration and repair (37, 38). Several studies have also used collagen and fibrin hydrogels as scaffolds to study lymphatic sprouting (28, 33). Helm et al. have shown that a fibrin-only matrix is optimal for LEC organization in vitro, compared with fibrin-collagen mixtures and collagen-only matrices (39). Fibrin

has also been widely used to support angiogenesis or to deliver growth factors. (40, 41). In addition, seeding LECs with adipose-derived stem cells (ADSCs) in a fibrin scaffold has been shown to induce the formation of a lymphatic network, suggesting that ADSCs and the fibrin hydrogel have a favorable effect on LEC differentiation (32). These data suggest that fibrin might promote lymphatic regeneration, motivating our studies to test its therapeutic potential after lymphatic injury.

To address this, we investigated whether fibrin scaffolding encourages the regeneration and repair of collecting lymphatics after injury. We developed a novel surgical mouse model to study lymphatic regeneration, demonstrating that resected segments of collecting vessels can be regenerated sufficiently after fibrin implantation, restoring lymph flow to the draining lymph node. Additionally, we observed that macrophages and neutrophils infiltrate the tissue surrounding injured lymphatic vessels and promote lymphatic regeneration in a CCL5-dependent manner. We show that depletion of these cells inhibits lymphatic regeneration. Our work motivates further translation of fibrin scaffolds to promote repair of lymphatic vessels after injury.

Results

Promotion of collecting lymphatic vessel sprouting are affected by fibrinogen concentration. Segments of collecting lymphatic vessels (~0.5 mm) were excised from the flanks of mice and cultured *in vitro* in a 3D fibrin scaffold using Opti-MEM media supplemented with 4% Ultroser G (a chemically semi-defined serum without VEGF-C) and under 5% O_2 and 5% CO_2 conditions. Only segments having outgrowths were used for quantitative analysis. When cultured *in vitro* in fibrin gel, lymphatic vessels sprouted over time (**Figure 1a-c**). Immunostaining of vessel segments from a PROX1-eGFP reporter mouse revealed that lymphatic sprouts express PROX1, podoplanin (PDPN), and α-SMA, indicating that both endothelial cells and lymphatic muscle cells contribute to the sprouts (**Supplementary Video 1**). Time-lapse imaging also revealed that on day 5, LMCs begin migrating along sprouts, and the fibrin gel breaks down as the sprouts extend around the explant. (**Figure 1b**, and **Supplementary Video 2**). The sprouting response changes as fibrinogen concentration increases (**Figure 1d, e**). Quantitative analysis of sprouts revealed that total sprout length significantly decreases with increasing fibrinogen concentration (n = 3 distinct vessels in each condition), from 17.2±4.2mm for 3mg/mL to 6.3±2.1mm for 15mg/mL (**Figure 1e**). There is a statistically significant difference in the total number of sprout endpoints between 9 mg/mL (233.7±27.2) and 15 mg/mL (77.5±16). Rheological testing also revealed that the gel's elastic properties changed significantly with an increase in fibrinogen concentration (**Figure 1e**). The storage modulus G′ was 555.1±38.7 (Pa) for 9mg/mL compared to 34.8±3.9 (Pa) for 3mg/mL and 1397.3±225.7 (Pa) for 15mg/mL, respectively (n=3). Vessels were only cultured for six days before analysis, as the results of vessel sprouting became highly variable after this point due to fibrin gel degradation. Based on explant sprouting responses, and mechanical properties at various fibrinogen concentrations, a concentration of 9 mg/mL was chosen for *in vivo* implantation.

Fibrin gel implantation promotes the regeneration of collecting vessels and restores lymphatic transport to the draining lymph node. To investigate whether fibrin scaffolding promotes lymphatic regeneration in vivo following lymphatic vessel

injury, we established a novel mouse model of lymphatic vessel injury in the hindlimb where 1-2 mm sections of the saphenous collecting lymphatic vessels were surgically resected without damaging the adjacent blood vessels (**Figure 2a**, **Supplementary Figure S1**, **Video S3**). A mixture of fibrinogen (9mg/ml final) and thrombin (2U/mL final) diluted in Opti-MEM was added to the injury site and allowed to polymerize to form fibrin *in situ* (**Supplementary Video S4**), or a sham injection was made. A representative NIR image shows reconnection of injured lymphatic vessels and lymph rerouting to the dermal lymphatics (**Figure 2b**). This reconnection did not occur in the absence of fibrin gel implantation. Confocal and fluorescence imaging using a PROX1-eGFP reporter mouse indicates sprouting of LECs at the injury site at week 3 post-injury in fibrin gel-implanted mice (**Figure 2c**). Confocal imaging also reveals lymphatic vessel sprouting at the site of vessel injury, as indicated by PDPN staining of collecting lymphatic vessels and αSMA staining of both lymphatic and blood vessel muscle cells (Supplementary **Figure S2**).

Representative longitudinal NIR imaging indicates that damaging collecting lymphatic vessels without gel implantation results in the loss of lymph transport to the draining lymph node, suggesting a lack of sufficient regeneration and repair following the damage (**Figure 2d, Videos S5 and S6**). By contrast, fibrin gel implantation restores lymphatic transport at the site of injury as early as two weeks post-gel implantation (**Figure 2d, Video S7**). In mice with injured lymphatic vessels, lymphatic vessel pumping—assessed by the frequency of vessel contractions proximal to the injury site (proximal packet frequency)—was significantly higher in the gel implantation group (average frequency = 7.89±1.96min^{-1} at week 2 and 7.34±1.90 min^{-1} at week 4) than the group with no gel (0±0 min^{-1} at week 2, and 0.41±0.41 min^{-1} at week 4). This suggests that gel implantation promotes lymphatic regeneration and restores pumping proximal to the injury site (**Figure 2e,** Supplementary **Figure S3**). However, gel implantation had no significant effect on the frequency of vessel contractions distal to the damaged site (distal packet frequency). NIR imaging from 4 weeks post-injury shows that animals with gel implantation are more likely to have their lymphatic flow restored and gain proximal filling (filling of lymphatic vessels proximal to the injury site) than mice without gel implantation ($p = 0.0256$, Fisher's Exact test; **Figure 2f**).

Next, we compared the lymph drainage between the control leg (contralateral leg with uninjured saphenous lymphatic vessels), the injured leg without gel implantation, and the injured leg with gel implantation by quantifying the accumulation of FITC-Dextran in the popliteal draining node and the inguinal lymph node, which is the next draining node that lymph could reach from the injection site in the mouse paw (**Figure 2g**). In the uninjured leg, the ratio of FITC fluorescence in the popliteal node to the inguinal node was ~5.6, suggesting the popliteal draining node has more than five times the amount of dye accumulation when compared to the inguinal node in the uninjured leg (**Figure 2h**). After injury, this ratio declines by almost 100-fold (from 5.60±1.19 to 0.054±0.01), implying that injuring collecting lymphatic vessels impedes lymph transport to the draining popliteal node (**Figure 2h**). Instead, the value of fluorescence in the inguinal node significantly increased ~4.3-fold, from 6.68±1.73 (a.u.) to 28.87±4.42 (a.u.), suggesting compensation by the collateral inguinal lymphatic route after saphenous lymphatic vessel injury. For the injured + gel group, the popliteal to inguinal fluorescence ratio is approximately one, corresponding to the average values of 16.89±3.24 (a.u.) and 16.81±2.99 (a.u.) for popliteal and inguinal nodes, respectively, suggesting that popliteal and inguinal routes equally contribute to lymph drainage after gel implantation. Overall, these results indicate that fibrin gel

implantation restores impaired lymphatic transport to draining lymph nodes following injury, with some redistribution of lymph between the inguinal and popliteal lymph nodes.

Macrophages and neutrophils infiltrate the tissue following lymphatic injury. To investigate whether macrophages and neutrophils infiltrate into the fibrin gel, we performed flow cytometry on the tissue surrounding the saphenous collecting lymphatic vessels 10 days after injury using CX3CR1+eGFP reporter mice. Flow cytometry using reporter mice revealed a significant increase in the percentage of F4/80(+) cells in the tissue after injury to the collecting lymphatic vessels (**Figure 3a,** Supplementary **Figure S4**). The data indicate the presence of two distinct macrophage phenotypes after lymphatic injury, with CCR2(+) macrophages infiltrating tissue in the absence of fibrin gel and CX3CR1(+) patrolling macrophages increasing with gel implantation (**Figures 3b**, **Supplementary Figure 6, Video S8**). We also performed a flow cytometry analysis using wild-type mice, which suggests that the macrophage population (CD11b+F4/80+) constitutes the majority of immune cell types within the leukocyte population in injured tissue (**Figures 3c and 3d**, Supplementary **Figure S5**). Notably, the percentage of macrophages significantly increased by approximately 50% after gel implantation compared to injury alone (from 42.0 ± 4.9 to 61.6 ± 1.3 for injury plus gel, $p<0.05$). Although neutrophils constitute a smaller portion of the immune cells in the tissue, there was a three-fold increase after gel implantation (from 1.4 ± 0.3 for the injury group to 4.1 ± 1.0 for injury plus gel, $p < 0.05$). Other immune cell types, such as NK, B, and T cells, as well as dendritic cells, showed no statistically significant changes post-gel implantation compared to the injury-only group (**Figure 3c and d**).

Local depletion of macrophages abrogates lymphatic regeneration after fibrin gel implantation. To test whether macrophage and neutrophil infiltrates contribute to lymphatic regeneration and pumping to restore function, we depleted macrophages and induced functional arrest of neutrophils locally using clodronate liposomes in mice with implanted fibrin gels after lymphatic vessel injury (**Figure 4a**). We compared functional NIR pumping metrics in mice treated with clodronate liposomes to those treated with control liposomes (**Figure 4b**, n = 4 per group). NIR imaging showed that clodronate treatment prevents lymphatic regeneration and the return of lymphatic contractions (**Figure 4c**). Lymphatic contractions were not observed proximal to the injury site after clodronate liposome treatment (proximal contraction frequency = 11.4±2.3 min^{-1} pre-surgery, 0±0 min^{-1} on days 14 and 28 following injury, gel implantation, and macrophage depletion), indicating impaired lymphatic regeneration. Additionally, distal packet frequency decreased by nearly tenfold (from 13.5±1.6 min^{-1} pre-surgery to 1.4±1.4 min^{-1} on day 14 and 1.3±1.3 min^{-1} on day 28). In the control liposome group, the pre-surgical packet frequency at the proximal injury site was not significantly different from the values on days 14 and 28 (from 9.5±1.8 min^{-1} pre-surgery to 7.9±2.9 min^{-1} on day 28), suggesting that lymphatic regeneration was not significantly affected by control liposome treatment.

NIR results from 4 weeks after treatment also show that mice treated with clodronate liposomes are less likely to gain proximal filling than mice without gel implantation ($p = 0.0256$, Fisher's Exact Test, **Figure 4d**). Confocal imaging after week 4 confirmed that macrophage depletion was successful, showing a nearly 10 fold decrease in $CX3CR^{GFP/+}$ cells at the surgical site in mice treated with clodronate liposomes (1707±305 cells per field of view (FOV) in the control liposomes group vs. 155±123

cells in the clodronate liposomes group; n=3 each group and FOV=1.6 mm^2; **Figure 4e**).

Fibrin gel implantation results in increased tissue CCL5 following lymphatic vessel injury, and genetic ablation of CCL5 inhibits regeneration. To determine which cytokines were upregulated as a result of lymphatic injury and gel implantation, we conducted a semi-quantitative cytokine array analysis on day 10 following lymphatic surgery and fibrin gel implantation. Interestingly, the array suggested that CCL5, but not CCL2 or CX3CL1, increased 31.6-fold after injury plus gel implantation, compared to a 9.6-fold increase for injury and a 10.3-fold increase for gel plus sham surgery, when normalized to the sham surgery group (**Figure 5a,** Supplementary **Figure S7**). Additionally, we observed an increase in the matrix metalloproteinase MMP-9 in mice with gel implantation after lymphatic injury (**Figure 5a,** Supplementary **Figure S7**). It is known that CCL5 functions as a ligand for CCR1, CCR3, and CCR5, attracting macrophages and T cells to the site of injury (34, 35). Thus, we set out to determine if genetic deletion of CCL5 inhibited lymphatic regeneration and the subsequent recovery of lymphatic pumping proximal to the injury site. In addition, the expression of CCR2 and CX3CR1 by infiltrating cells prompted us to determine if a deficiency in CCR2 or CX3CR1 impairs lymphatic regeneration. We also tested whether VEGF-C was upregulated after gel implantation in mice with lymphatic injury. There was no difference in tissue VEGF-C between gel+injury and injury groups (**Supplementary Figure 8**)

Non-invasive NIR imaging of lymphatic function 4 weeks after injury showed that mice lacking CCL5 are less likely than control mice to recover their proximal filling (filling of lymphatic vessels proximal to the injury site) following gel implantation (p=0.0498, Fisher's Exact test; **Figure 5b**). However, filling of the proximal lymphatic vessel with NIR dye was not different in the double mutant *Cx3cr1* and *Ccr2* mouse model ($CCR2^{RFP/RFP}CX3CR1^{GPP/GFP}$) compared to control mice. This suggests that CX3CR1 and CCR2 are critical for regeneration 4 weeks after injury and gel implantation (p = 0.5105, Fisher's Exact Test). Interestingly, confocal imaging shows that cells expressing CX3CR1 and CCR2 still infiltrate tissue in $CCR2^{RFP/RFP}$ $CX3CR1^{GPP/GFP}$ mice, indicating that neither CCR2 nor CX3CR1 is responsible for recruiting those cells (**Supplementary Figure S9**), and suggesting these receptors are not involved in the trafficking of macrophages to the site of injury. Surprisingly, CCL5-deficient mice also maintained macrophage and neutrophil infiltration (**Figures 3c and 3d**). Furthermore, NIR imaging two weeks after surgery showed a significant decrease in proximal pumping frequency in CCL5 knockout mice and double-deficient CX3CR1 and CCR2 mice compared to mice deficient in only CCR2 or CX3CR1, as well as wild-type mice **(Figure 5c). T**he difference in post-injury pumping frequency observed two weeks post-injury was no longer present four weeks after injury.

Discussion

Disruption of lymphatic function due to cancer surgery, radiation therapy, traumatic injuries, or infection is a common cause of secondary lymphedema (36). The notion is that lymphedema is caused by an inadequate lymphatic regeneration, leading to subsequent pumping dysfunction after cancer surgery and therapy, which manifests as fluid accumulation in soft tissues. (79). Our major finding is that implanting a fibrin hydrogel with appropriate fiber density and mechanical properties after lymphatic vessel injury leads to lymphatic regeneration and restoration of lymphatic flow to the

draining lymph node as early as two weeks post-gel implantation (80). The results revealed that LECs sprouted from injured collecting lymphatic vessels to reconnect injured vessels. In addition, our results show other compensation of the adjacent lymphatic networks, including the re-routing of lymph transport to other nodes after the primary lymph drainage route is injured. Additionally, a collateralization response redirects lymph flow to dermal lymphatics, partially compensating for the reduced transport of lymphatic fluid through collecting vessels after injury.

Fibrin has been widely used to support angiogenesis or to deliver growth factors. (40, 41). Studies have also shown that fibrin hydrogels promote LEC differentiation, sprouting and organization (28, 33)(39)(32). In a porcine lymphedema model, implanting nano-fibrillar collagen scaffolds has been reported to increase lymphatic vessel density (31). Consistent with earlier studies, our findings indicate that the fibrin scaffold effectively supports lymphatic regeneration. When cultured on soft matrix, LECs are known to express more genes associated with cell migration (42). Our data also show sprouting responses tend to decrease at higher fibrinogen concentrations, with the optimal sprouting response occurring at a concentration of 9 mg/mL, corresponding to a storage modulus (G') of 555 Pa. *In* vitro sprouting of collecting lymphatic vessels revealed the presence of PDPN (+) cells, accompanied by partial coverage by SMA (+) cells, indicating that the sprouts contain both LECs and LMCs. Immunostaining of saphenous tissue, four weeks after collecting vessel injury and gel implantation, also confirmed sprouts at the site of collecting lymphatic vessel injury, expressing PDPN with partial SMA coverage.

We also found that two distinct macrophage phenotypes infiltrate the tissue after collecting lymphatic vessel injury: i) CCR2+ macrophages increase in the tissue after injury without gel implantation, and ii) CX3CR1+ patrolling macrophages infiltrate the tissue after fibrin gel implantation. Our findings suggest that macrophages expressing CX3CR1(+) infiltrate the fibrin gel and accumulate in proximity to regenerating lymphatic vessels. In general, monocytes and monocyte-derived macrophages have been reported to express CCR2 and CX3CR1 receptors, with inflammatory monocytes expressing high levels of LY6C and CCR2 (CX3CR1low) and patrolling/reparative monocytes expressing high levels of CX3CR1 (CCR2low LY6Clow) (43). Earlier investigations have also reported that CCR2(+) and double-positive CCR2 and CX3CR1 macrophages infiltrate fibrin implants, contributing to fibrin endocytosis and clearance (44). Additionally, tissue-resident macrophages expressing CX3CR1 have been demonstrated to regulate lymphatic vessel growth in cardiac lymphatic vessels through direct interaction with LECs (45). Similarly, embryos lacking macrophages have been shown to develop malformed lymphatic vessels, suggesting that macrophages play a crucial role in lymphatic morphogenesis (46). It has also been established via fate-mapping that CX3CR1+ cells are tissue-resident macrophages originating embryonically from the yolk sac or fetal liver, and postnatally from the bone marrow (47). Interestingly, we found that the deficiency in CCR2 or CX3CR1 function did not significantly inhibit macrophage infiltration and lymphatic regeneration into the fibrin gels after lymphatic injury. Consistent with this observation, previous research has suggested that LY6Clow patrolling/reparative monocytes rely on CCR5, but not CCR2 or CX3CR1, to migrate to the injury site (48). CCL5, expressed by endothelial cells and activated leukocytes, is a potent chemoattractant for monocytes and lymphocytes acting via CCR1 and CCR5 receptors (34, 35). Upon stimulation, LECs and LMCs have been shown to secrete CCL5 chemokine (49, 50). Mice lacking CCL5 have also been

reported to exhibit impaired monocyte recruitment and T cell function, as well as significantly reduced swelling in the delayed-type hypersensitivity assay (51). Notably, we found that CCL5, but not CCL2, CCL3, or CX3CL1, is markedly elevated with the implantation of fibrin gel after lymphatic injury. Our data suggest that many immune cell types within the injured tissue, including T lymphocytes, macrophages, NK cells, neutrophils, and dendritic cells, express CCR5. However, the genetic deletion of CCL5 did not result in a statistically significant decline of CCR5+ cell infiltration within these populations. This suggests that CCL5 alone does not orchestrate the recruitment of these cells following gel implantation. It is worth noting that CCL5 has been shown to control a multitude of cellular functions beyond chemotaxis, such as cell survival, proliferation, and apoptosis (52–54). Thus, rather than recruiting CCR5+ cells to the injury site, the elevated CCL5 in our system may be directly supporting the local repair process by affecting the phenotype of the CCR5+ cells. One limitation of the CCL5-KO approach is that CCR5 interacts with other ligands such as CCL3, CCL4, and CCL3L1, which may be involved in compensatory mechanisms for cell recruitment.

We also observed that genetic ablation of CCL5 impairs the lymphatic regeneration process. In this regard, CCL5 may contribute to lymphatic regeneration in several ways. Monocytes have been demonstrated to increase MMP-9 production in response to CCL5 stimulation (55). MMP-9 cleaves ECM-bound growth factors and degrades type IV collagen in the basement membrane, allowing increased endothelial migration and sprouting (56). We also found that MMP9 was highly elevated after fibrin gel implantation, suggesting that CCL5 could be involved in MMP-9 upregulation (**Figure 5a**, Supplementary **Figure S7**). Aside from being a chemokine for monocytes, CCL5 is also known to recruit endothelial progenitor cells—c-Kit+Tie-2+ cells expressing CCR5—from the circulation to promote neovascularization at the site of injury (57). A subset of mesenteric LECs has also been reported to originate from cKit+ hemogenic endothelial cells (58). In addition, CCL5 may play a role in VEGF-C production, as CCL5 has been reported to induce VEGF-C production in human chondrosarcoma cells (59). The VEGF-C/VEGFR-3 signaling pathway is known to be an important regulator of PROX1+ cell sprouting during development, as well as lymphangiogenesis in the context of cancer and inflammation(60–64). Previous research has shown that VEGF-C enhances lymphatic sprouting from 3D-cultured lymphatic vessel segments, but its inhibition via either soluble VEGFR-3 or the VEGFR-3 kinase inhibitor MAZ51 only partially reduces lymphatic sprouting (28). Our ELISA experiments indicate that VEGF-C levels are less than 0.3 ng/µg of total protein and do not differ between any groups. We also found that collecting lymphatic vessel explants cultured in a 3D fibrin hydrogel without exogenous growth factor supplementation promotes lymphatic sprouting in vitro. Growth factors such as VEGF-C and VEGF-D can bind to VEGFR3 with high affinity, and VEGFR3 can also be activated independently of growth factors through lymphatic flow (65). Our observation aligns with other in vitro studies where lymphatic vessels sprouted without exogenous VEGF-C supplementation (29). Similarly, it has been shown that blood endothelial cells (BECs) in aortic ring assays sprout in collagen and fibrin matrices without the addition of angiogenic growth factors such as VEGF or bFGF. Our results suggest that similar mechanisms are engaged when LECs contact fibrin gels produced during injury (or added exogenously, as in the current work). For blood vessel ECs, the type of matrix appears to influence the response to growth factors; for example, VEGF enhances angiogenesis in a collagen gel, while fibrin supports sprouting in response to bFGF (66). Further studies are needed to investigate similar synergies in lymphatic regeneration. Our in vivo data suggest that increased VEGF-C levels are not associated with the observed lymphatic regeneration.

Limitations and Future Directions

One limitation of our study is that the injury model does not induce edema, which limits our ability to study the benefit of gel implantation in preventing lymphedema. In humans, lymphedema occurs in a delayed fashion, months to years following lymphatic damage caused by cancer treatment (67). In contrast, swelling caused by damage to lymphatic vessels and skin in mice resolves on its own if given enough time (68, 69). In agreement with previous studies, we also did not observe persistent swelling following popliteal lymphatic damage. One potential explanation is that the mouse models cannot fully recapitulate lymphatic pathophysiology, such as the effect of gravitational dependence on lymphedema progression. Further, a recent report suggests that injury in sheep hindlimbs doesn't lead to lymphedema and that collecting lymphatic vessels may spontaneously regenerate following injury (70). This is in contrast to our finding that, in the absence of scaffolding, collecting lymphatic vessels do not adequately regenerate to reconnect injured lymphatic vessels. This disparity could be due to the severity of the injury to the hindlimb of a sheep, where the lymphatic excision was relatively small. In our injury model, we remove 2 mm of lymphatic vessel, while leaving the draining lymph node intact. Moreover, differences in the preexisting lymphatic network in the hindlimbs of mice and sheep, which can influence how lymph transverses to the preexisting network of lymphatic pre-collectors, may account for the observed disparity. It is essential to acknowledge that our approach for depleting macrophages with clodronate also leads to the functional arrest of neutrophils (71). While macrophages constitute the majority of infiltrating cells and significantly increase after gel implantation, neutrophils—which make up <5% of immune cells within the tissue—also increase after injury and gel implantation when compared to the injury group. Neutrophils, the most abundant immune cells, play a central role in the initial phase of the immune response following injuries (72). Recent evidence suggests that neutrophils significantly contribute to tissue repair and the resolution of inflammation by producing angiogenic factors and proteases, such as MMP-9 (72). Thus, neutrophils may also be playing a critical role in the fibrin-induced lymphatic regeneration.

Previous research has shown that VEGF-C chemically incorporated into fibrin induces local lymphangiogenesis, affecting only initial lymphatics and not the collecting lymphatic vessels, with fibrin alone failing to induce lymphangiogenesis (73). In our experiments, where we specifically injured collecting lymphatic vessels, we observed that fibrin alone was sufficient to induce lymphatic sprouting, both in vivo and in vitro. This discrepancy may be due to the unique design of our injury model, which targets collecting lymphatic vessels, in contrast to the previous study that focused on initial lymphatics within the mouse ear. While our study primarily focused on the effect of fibrin on immune cell recruitment, the fibrin gel effect may extend beyond these areas and influence various pro- and anti-lymphangiogenic factors such as the VEGF-C-VEGFR3 axis. For example, the proteome profile analysis suggests a decrease in the antiangiogenic factor SERPINF1 which warrants further investigation. Another limitation is that our animal model does not allow for high-resolution longitudinal imaging to understand the dynamics of lymphatic regeneration in vivo. Future studies

should aim to develop animal models equipped with chronic imaging windows to overcome this limitation.

Materials and Methods

Mice. C57BL/6 mice, and αSMA-DsRed (C57BL/6) were obtained from the Cox-7 animal facility operated by the Edwin L. Steele Laboratories, Department of Radiation Oncology at MGH. PROX1-eGFP (kind gift of Taija Mäkinen, Uppsala University, and Young-Kwon Hong, University of Southern California), CX3CR1$^{GFP/+}$ and CX3CR1$^{GFP/+}$CCR2$^{RFP/+}$ reporter mice (C57BL/6, JAX), double mutant CX3CR1$^{GFP/RFP}$CCR2$^{RFP/RFP}$ mice (C57BL/6, JAX), and CCL5-KO mice (C57BL/6, JAX) were housed in MGH Center for Comparative Medicine facilities. Female and male mice (8–20 weeks old) were used in this study. Animal protocols were approved by the Institutional Animal Care and Use Committees (IACUC) at MGH, and all facilities are accredited by the Association for Assessment and Accreditation of Laboratory Animal Care International (AAALAC). All methods were performed in accordance with the relevant AAALAC recommendations and the ARRIVE guidelines. Mice were euthanized with an overdose of FATAL-PLUS (pentobarbital sodium; 1 mL/kg body weight, intraperitoneal injection), followed by cervical dislocation to confirm death. All procedures were approved by the Institutional Animal Care and Use Committee (IACUC) at Massachusetts General Hospital (MGH) and were in accordance with the American Veterinary Medical Association (AVMA) Guidelines for the Euthanasia of Animals.

Lymphatic injury surgical procedure. Mice were anesthetized with the administration of ketamine (10 mg/kg) and xylazine (100 mg/kg). To enhance the visibility of lymphatic vessels, 5 µL of Evans Blue (0.1% diluted in PBS) was injected into the mouse footpad. Fur was removed by shaving and applying a depilatory cream. To gain access to two saphenous lymphatic vessels—the afferent collecting lymphatic vessels to the popliteal lymph node—that run along the saphenous vein, a skin incision distal to the knee in the mouse hindlimb was made using a scalpel. A small segment of the saphenous lymphatic vessel (1-2 mm) was excised using a microsurgical scissor and under a stereomicroscope. Care was taken to prevent damage to the saphenous vein, and mice with bleeding were excluded. For the gel implantation studies, ~10 µL of unpolymerized fibrin gel (a mixture of fibrinogen, 9mg/ml final concentration and thrombin, 2U/mL final concentration, diluted in Opti-MEM) was added to the injury site by pipette. Once the procedure was completed, the incision site was sutured (number 5-0, Ethicon). Buprenorphine (0.05-0.1 mg/kg) was used post-operatively as an analgesic.

3D lymphatic vessel culture in fibrin gel. Segments of collecting lymphatic vessels were embedded in a fibrin gel in a 48-well plate. Briefly, fibrinogen (Sigma, cat#F8630) was diluted in Opti-MEM (Gibco, cat#31985062) to yield the desired concentration. The solution was incubated for at least one hour at 37 °C to dissolve, and then it was filtered (0.22 µm) to remove unpolymerized fibrinogen. Aliquots of fibrinogen solutions (30 mg/mL, 18mg/mL, and 6mg/mL) were placed on ice. Thrombin (Sigma cat#T4648) at 4U/mL was added to each fibrinogen aliquot (1:1 ratio) to begin the polymerization of fibrinogen into fibrin strands immediately. Segments of collecting lymphatic vessels were encapsulated between two 200uL fibrin layers in a 48-well plate. After polymerization, 800uL of MCDB 131 Medium (Gibco, cat# 10372019), supplemented

with 4% Ultroser™ G serum substitute, 1% hydrocortisone (STEMCELL Technologies, cat# 74142), 1% L-Glutamine (Gibco™), 1% Penicillin-Streptomycin (Gibco™), was used to culture segments under 5%O_2 and 5%CO_2 for six days (28).

Fibrin rheological measurement. Fibrin elastic properties were measured using an oscillatory shear rheometer (AR-G2, TA Instruments, DE) as described previously (74, 75). In brief, a 40-mm-diameter parallel plate was used, and the plate temperature was maintained at 37 °C throughout the measurement. The unpolymerized fibrin precursor solution was pipetted onto the bottom plate of the rheometer before the top plate was lowered to a gap of 500 μm such that the solution completely filled the space between the two plates. With a moisture trap placed around the plates, the fibrin hydrogel was allowed to polymerize for 15 minutes. After polymerization, a frequency sweep test was performed with 1% strain over a frequency range of 0.1–100 Hz. Three replicates were tested for each gel concentration. Measurements at 1 Hz were used to compare storage modulus (G') values at different gel concentrations.

FITC-Dextran uptake experiment. 10μL of 1% FITC-Dextran (40,000 MW, Sigma) in PBS was injected into the dorsal aspect of the mouse paw. Popliteal and inguinal lymph nodes were harvested 3 hours after the injection. Each node was homogenized in 1mL of PBS using a tissue homogenizer. 300uL of each sample was transferred to a 96-well plate, and fluorescence was measured using a Fluorescent Ascent™ Fluorometer (Thermo Scientific).

Near-infrared imaging. Lymphatic near-infrared imaging (NIR) was used to assess lymphatic pumping and regeneration in vivo. Mice were anesthetized with ketamine/xylene. Hair was removed using a depilatory cream, and 5μL of Dextran (10K), Flamma® 774 (BioActs), was injected intradermally into the dorsal aspect of the mouse paw. To image the saphenous afferent lymphatic vessels, near-infrared imaging was performed using a previously described NIR setup (76). Briefly, the imaging system is composed of a ×6.5 Zoom lens (Navitar) and a Prosilica GT2750 camera (Allied Vision Technology) with an ICG-B emission filter (832/37, Semrock). A custom-built ring light source was used to excite the dye using 760 nm high-power laser-emitting diodes (Marubeni) filtered through a 775/50 bandpass filter (Chroma). A custom-written MATLAB code was used to analyze images.

Macrophage and neutrophil depletion experiment. Clodronate liposomes and control liposomes were purchased from Liposoma BV. Fibrin gel was prepared by mixing a 1:1 ratio of fibrinogen (18mg/mL) and thrombin solution (4U/mL) as described previously. After ligating afferent popliteal lymphatic vessels in CX3CR1$^{GFP/+}$ mice, liposomes (10% v/v) were immediately added to the fibrin gel before polymerization, and 10μL of fibrin gel loaded with clodronate liposomes was implanted at the injury site. Subcutaneous injection of 10μL of clodronate liposomes at the injury site was repeated at 3, 7, 14, and 21 days after gel implantation. In control experiments, control liposome (10% v/v) was added to the fibrin gel, and subcutaneous injections of control liposome were repeated on days 3, 7, 14, and 21 after surgery and gel implantation. NIR functional lymphatic imaging was performed ~3-4 days before surgery and at 2- and 4-weeks post-surgery. Finally, popliteal tissues from CX3CR1$^{GFP/+}$ mice were harvested, and confocal imaging was performed to confirm macrophage depletion by clodronate liposomes.

Single cell suspension and flow cytometry. To prepare a single-cell suspension, saphenous tissue, including saphenous lymphatic vessels afferent to the popliteal lymph node, were dissected from individual mice. Harvested tissues were placed on ice-cold DMEM 1X (Corning, with 4.5 g/L glucose, L-glutamine & sodium pyruvate), minced with a surgical scalpel and fine forceps. Minced tissues were transferred into 5mL test tubes containing 2 mL of freshly made enzyme mix containing (0.8 mg/mL Dispase II (Sigma), 0.2 mg/mL Collagenase P (Roche), and 0.01mg/mL DNase (Roche). Samples were incubated at 37˚ C with gentle rocking for 30 minutes. Following incubation with the enzyme mix, the digested tissue was aspirated using a 1-mL pipette, 3 mL of DMEM 1X was added to the mixture, which was then filtered through a 70 µm nylon mesh. The mixture was centrifuged (1500 rpm, 5 min at 4 ºC), the supernatant was decanted, and the cell pellet was resuspended in 200µL of ice-cold FACS buffer (1% BSA in PBS). The cells were blocked using anti-CD16/32 antibodies. Cell surface markers were stained for 20 minutes on ice (see Table S1 for a list of antibodies). Flow cytometry was performed with FACSAria (B.D. Biosciences). Data analysis was performed via FlowJo (Tree Star).

Proteome Profiler Cytokine Array and ELISA. Proteome profiler cytokine array (R&D systems, Minneapolis, MN) was used to screen relative levels of inflammatory cytokines following lymphatic injury and gel implantation according to the manufacturer's protocol. There were four groups, as follows (i) sham injury: in the sham group, a skin incision was made without injuring lymphatic vessels; (ii) lymphatic injury: in the injury group, a section of saphenous afferent lymphatic vessel to the popliteal lymph node was surgically removed, but the gel was not implanted; (iii) sham injury plus gel, a skin incision was made with a scalpel, gel was implanted at the site of the injury without injuring lymphatic vessels; (iv) injury plus gel, a section of saphenous afferent lymphatic vessel to the popliteal lymph node was surgically removed and the fibrin gel was implanted. After 10 days, tissues were harvested from the saphenous region and homogenized using a handheld homogenizer according to the manufacturer's protocol. Tissue lysates were used for cytokine arrays, as directed by the manufacturer. Cytokine expression was semi-quantitively determined via densitometric analysis by Protein Array Tool in MATLAB (77). The data were presented as fold-change in comparison to the sham group (see **Figure S7** for array images). Human VEGF-C DuoSet ELISA (DY293B) was used to detect VEGFC levels.

Immunostaining. Lymphatic sprouts from *in vitro* culture were fixed for 30 minutes in 4% PFA (vol/vol) at room temperature. The sprouts were washed three times with PBS and placed in 10% donkey serum and 0.5% Triton X-100 in PBS for 1 hour at room temperature. After incubation with the podoplanin (PDPN) antibody overnight at 4 °C, segments were washed with PBS and incubated with the secondary antibody, or αSMA-Cy3, overnight at 4 °C. After washing with PBS three times, the segments were placed on the microscope slide to perform imaging. For staining with lectin, segments were incubated with diluted lectin (1:100) overnight after fixation. For wholemount staining of collecting lymphatic vessels from mice with PDPN, 10 µL of diluted PDPLN in PBS (1:50) and FcBlock (1:500) were injected into the mouse footpad. After 24 hours, 10 µL of diluted secondary antibody was injected into the mouse foot. The popliteal tissue was then harvested after 1 hour. For lectin whole-mount staining, 10 µL of diluted lectin was injected into the mouse footpad, and tissue was harvested 1~2 hours after the injection. For αSMA or F4/80 whole-mount staining, the popliteal tissue was fixed with 4% PFA for 30 minutes, washed with PBS, and incubated with conjugated antibody overnight at 4°C. After washing, the tissue was placed on a glass slide to visualize

lymphatic vessels under a confocal microscope. Please see Supplementary Table 1 for details on the antibodies.

Software and Statistical analysis. AngioTools Software and Neurite-J plugin were used to measure various morphometric parameters of lymphatic sprouts (78, 79). In brief, Nurite-J and ImageJ were used for image segmentation. Angiotools was used to quantify morphometric parameters. To analyze confocal images and quantify cells based on fluorescence staining, the Colocalization Object Counter plugin in FIJI was used (80). A custom-written MATLAB script was used to analyze NIR data and obtain lymphatic pumping metrics (68). Schematic figures were created with BioRender. All statistical analysis was performed in Prism 9. Statistical significance was tested using a one-way ANOVA with the Tukey post hoc test or a two-tailed Student's t-test, as appropriate. To test if there is a nonrandom association between categorical data (e.g., test if there is an association between gel implantation and the success of regeneration), Fisher’s Exact test was used. The significance was set at $P<0.05$.

References

1. M. A. Swartz, The physiology of the lymphatic system. *Adv Drug Deliver Rev* **50**, 3–20, (2001).

2. D. C. Zawieja, Contractile Physiology of Lymphatics. *Lymphat. Res. Biol.* **7**, 87–96, (2009).

3. J. T. Wigle, G. Oliver, Prox1 Function Is Required for the Development of the Murine Lymphatic System. *Cell* **98**, 769–778, (1999).

4. M. J. Karkkainen, *et al.*, Vascular endothelial growth factor C is required for sprouting of the first lymphatic vessels from embryonic veins. *Nat Immunol* **5**, 74–80, (2004).

5. I. Martínez-Corral, *et al.*, In vivo imaging of lymphatic vessels in development, wound healing, inflammation, and tumor metastasis. *Proc National Acad Sci* **109**, 6223–6228, (2012).

6. W. Zheng, A. Aspelund, K. Alitalo, Lymphangiogenic factors, mechanisms, and applications. *J Clin Invest* **124**, 878–887, (2014).

7. K. Radhakrishnan, S. G. Rockson, The Clinical Spectrum of Lymphatic Disease. *Ann Ny Acad Sci* **1131**, 155–184, (2008).

8. S. G. Rockson, K. K. Rivera, Estimating the Population Burden of Lymphedema. *Ann. N. York Acad. Sci.* **1131**, 147–154, (2008).

9. D. Jones, *et al.*, Methicillin-resistant Staphylococcus aureus causes sustained collecting lymphatic vessel dysfunction. *Sci Transl Med* **10**, eaam7964, (2018).

10. S. G. Rockson, V. Keeley, S. Kilbreath, A. Szuba, A. Towers, Cancer-associated secondary lymphoedema. *Nat Rev Dis Primers* **5**, 22, (2019).

11. S. G. Rockson, Lymphedema after Breast Cancer Treatment. *N. Engl. J. Med.* **379**, 1937–1944, (2018).

12. A. J. M. Cornelissen, *et al.*, Lymphatico-venous anastomosis as treatment for breast cancer-related lymphedema: a prospective study on quality of life. *Breast Cancer Res Tr* **163**, 281–286, (2017).

13. A. Raju, D. W. Chang, Vascularized Lymph Node Transfer for Treatment of Lymphedema. *Ann Surg* **261**, 1013–1023, (2015).

14. T. Ozmen, M. Lazaro, Y. Zhou, A. Vinyard, E. Avisar, Evaluation of Simplified Lymphatic Microsurgical Preventing Healing Approach (S-LYMPHA) for the Prevention of Breast Cancer–Related Clinical Lymphedema After Axillary Lymph Node Dissection. *Ann Surg* **Publish Ahead of Print**, NA;, (2018).

15. A. Yan, T. Avraham, J. C. Zampell, S. Z. Aschen, B. J. Mehrara, Mechanisms of Lymphatic Regeneration after Tissue Transfer. *Plos One* **6**, e17201, (2011).

16. T. P. Viitanen, *et al.*, Lymphatic Vessel Function and Lymphatic Growth Factor Secretion after Microvascular Lymph Node Transfer in Lymphedema Patients. *Plastic Reconstr Surg Global Open* **1**, 1–9, (2013).

17. K. Watari, *et al.*, Tumor-Derived Interleukin-1 Promotes Lymphangiogenesis and Lymph Node Metastasis through M2-Type Macrophages. *Plos One* **9**, e99568, (2014).

18. J. C. Zampell, *et al.*, CD4+ Cells Regulate Fibrosis and Lymphangiogenesis in Response to Lymphatic Fluid Stasis. *Plos One* **7**, e49940, (2012).

19. K. Maruyama, *et al.*, Inflammation-induced lymphangiogenesis in the cornea arises from CD11b-positive macrophages. *J Clin Invest* **115**, 2363–2372, (2005).

20. S. F. Schoppmann, *et al.*, Tumor-Associated Macrophages Express Lymphatic Endothelial Growth Factors and Are Related to Peritumoral Lymphangiogenesis. *Am J Pathology* **161**, 947–956, (2002).

21. S. A. Stacker, M. G. Achen, L. Jussila, M. E. Baldwin, K. Alitalo, Lymphangiogenesis and cancer metastasis. *Nat Rev Cancer* **2**, 573–583, (2002).

22. J. C. Gardenier, *et al.*, Diphtheria toxin–mediated ablation of lymphatic endothelial cells results in progressive lymphedema. *Jci Insight* **1**, e84095, (2016).

23. J. C. Gardenier, *et al.*, Topical tacrolimus for the treatment of secondary lymphedema. *Nat Commun* **8**, 14345, (2017).

24. W. Tian, *et al.*, Leukotriene B4 antagonism ameliorates experimental lymphedema. *Sci Transl Med* **9**, (2017).

25. P. Baluk, *et al.*, TNF-α drives remodeling of blood vessels and lymphatics in sustained airway inflammation in mice. *J Clin Invest* **119**, 2954–2964, (2009).

26. P. Baluk, *et al.*, Transgenic Overexpression of Interleukin-1β Induces Persistent Lymphangiogenesis But Not Angiogenesis in Mouse Airways. *Am J Pathology* **182**, 1434–1447, (2013).

27. A. Ristimäki, K. Narko, B. Enholm, V. Joukov, K. Alitalo, Proinflammatory Cytokines Regulate Expression of the Lymphatic Endothelial Mitogen Vascular Endothelial Growth Factor-C*. *J Biol Chem* **273**, 8413–8418, (1998).

28. F. Bruyère, *et al.*, Modeling lymphangiogenesis in a three-dimensional culture system. *Nat. Methods* **5**, 431–437, (2008).

29. J. S. T. Hooks, *et al.*, Synthetic hydrogels engineered to promote collecting lymphatic vessel sprouting. *Biomaterials*, 121483, (2022), https:/doi.org/10.1016/j.biomaterials.2022.121483.

30. T. Tammela, *et al.*, Therapeutic differentiation and maturation of lymphatic vessels after lymph node dissection and transplantation. *Nat Med* **13**, 1458–1466, (2007).

31. C. Hadamitzky, *et al.*, Aligned nanofibrillar collagen scaffolds – Guiding lymphangiogenesis for treatment of acquired lymphedema. *Biomaterials* **102**, 259–267, (2016).

32. L. Knezevic, *et al.*, Engineering Blood and Lymphatic Microvascular Networks in Fibrin Matrices. *Frontiers Bioeng Biotechnology* **5**, 25, (2017).

33. D. Marino, J. Luginbühl, S. Scola, M. Meuli, E. Reichmann, Bioengineering Dermo-Epidermal Skin Grafts with Blood and Lymphatic Capillaries. *Sci Transl Med* **6**, 221ra14, (2014).

34. T. J. Schall, K. Bacon, K. J. Toy, D. V. Goeddel, Selective attraction of monocytes and T lymphocytes of the memory phenotype by cytokine RANTES. *Nature* **347**, 669–671, (1990).

35. T. T. Murooka, R. Rahbar, L. C. Platanias, E. N. Fish, CCL5-mediated T-cell chemotaxis involves the initiation of mRNA translation through mTOR/4E-BP1. *Blood* **111**, 4892–4901, (2008).

36. A. Szuba, S. G. Rockson, Lymphedema: classification, diagnosis and therapy. *Vasc Med* **3**, 145–156, (1998).

37. P. S. Ciano, R. B. Colvin, A. M. Dvorak, J. McDonagh, H. F. Dvorak, Macrophage migration in fibrin gel matrices. *Laboratory Investigation J Technical Methods Pathology* **54**, 62–70, (1986).

38. N. LAURENS, P. KOOLWIJK, M. P. M. D. MAAT, Fibrin structure and wound healing. *J Thromb Haemost* **4**, 932–939, (2006).

39. C. E. Helm, A. Zisch, M. A. Swartz, Engineered blood and lymphatic capillaries in 3-D VEGF-fibrin-collagen matrices with interstitial flow. *Biotechnol Bioeng* **96**, 167–176, (2007).

40. J. S. Jeon, *et al.*, Human 3D vascularized organotypic microfluidic assays to study breast cancer cell extravasation. *Proc. Natl. Acad. Sci.* **112**, 214–219, (2015).

41. A. H. Zisch, U. Schenk, J. C. Schense, S. E. Sakiyama-Elbert, J. A. Hubbell, Covalently conjugated VEGF–fibrin matrices for endothelialization. *J. Control. Release* **72**, 101–113, (2001).

42. M. Frye, *et al.*, Matrix stiffness controls lymphatic vessel formation through regulation of a GATA2-dependent transcriptional program. *Nat Commun* **9**, 1511, (2018).

43. C. Shi, E. G. Pamer, Monocyte recruitment during infection and inflammation. *Nat Rev Immunol* **11**, 762–774, (2011).

44. M. P. Motley, *et al.*, A CCR2 macrophage endocytic pathway mediates extravascular fibrin clearance in vivo. *Blood* **127**, 1085–1096, (2016).

45. T. J. Cahill, *et al.*, Tissue-resident macrophages regulate lymphatic vessel growth and patterning in the developing heart. *Development* **148**, dev194563, (2021).

46. E. J. Gordon, *et al.*, Macrophages define dermal lymphatic vessel calibre during development by regulating lymphatic endothelial cell proliferation. *Development* **137**, 3899–3910, (2010).

47. S. Ensan, *et al.*, Self-renewing resident arterial macrophages arise from embryonic CX3CR1+ precursors and circulating monocytes immediately after birth. *Nat. Immunol.* **17**, 159–168, (2016).

48. F. Tacke, *et al.*, Monocyte subsets differentially employ CCR2, CCR5, and CX3CR1 to accumulate within atherosclerotic plaques. *J Clin Invest* **117**, 185–194, (2007).

49. L. A. Johnson, D. G. Jackson, The chemokine CX3CL1 promotes trafficking of dendritic cells through inflamed lymphatics. *J Cell Sci* **126**, 5259–5270, (2013).

50. K. M. Lee, *et al.*, D6 facilitates cellular migration and fluid flow to lymph nodes by suppressing lymphatic congestion. *Blood* **118**, 6220–6229, (2011).

51. Y. Makino, *et al.*, Impaired T Cell Function in RANTES-Deficient Mice. *Clin Immunol* **102**, 302–309, (2002).

52. D. J. Dairaghi, *et al.*, RANTES-Induced T Cell Activation Correlates with CD3 Expression. *J. Immunol.* **160**, 426-433, (1998).

53. R. K. Ganju, *et al.*, β-Chemokine Receptor CCR5 Signals Via the Novel Tyrosine Kinase RAFTK. *Blood* **91**, 791–797, (1998).

54. K. B. Bacon, B. A. Premack, P. Gardner, T. J. Schall, Activation of Dual T Cell Signaling Pathways by the Chemokine RANTES. *Science* **269**, 1727–1730, (1995).

55. S. C. Robinson, K. A. Scott, F. R. Balkwill, Chemokine stimulation of monocyte matrix metalloproteinase-9 requires endogenous TNF-alpha. *Eur J Immunol* **32**, 404–12, (2002).

56. G. Bergers, *et al.*, Matrix metalloproteinase-9 triggers the angiogenic switch during carcinogenesis. *Nat Cell Biol* **2**, 737–744, (2000).

57. Y. Ishida, *et al.*, Pivotal role of the CCL5/CCR5 interaction for recruitment of endothelial progenitor cells in mouse wound healing. *J Clin Invest* **122**, 711–721, (2012).

58. L. Stanczuk, *et al.*, cKit Lineage Hemogenic Endothelium-Derived Cells Contribute to Mesenteric Lymphatic Vessels. *Cell Reports* **10**, 1708–1721, (2015).

59. L.-H. Wang, *et al.*, CCL5 promotes VEGF-C production and induces lymphangiogenesis by suppressing miR-507 in human chondrosarcoma cells. *Oncotarget* **7**, 36896–36908, (2016).

60. M. Skobe, *et al.*, Induction of tumor lymphangiogenesis by VEGF-C promotes breast cancer metastasis. *Nat. Med.* **7**, 192–198, (2001).

61. H. Ji, *et al.*, TNFR1 mediates TNF-α-induced tumour lymphangiogenesis and metastasis by modulating VEGF-C-VEGFR3 signalling. *Nat. Commun.* **5**, 4944, (2014).

62. H. Kim, R. P. Kataru, G. Y. Koh, Inflammation-associated lymphangiogenesis: a double-edged sword? *J. Clin. Investig.* **124**, 936–942, (2014).

63. R. S. Srinivasan, *et al.*, Lineage tracing demonstrates the venous origin of the mammalian lymphatic vasculature. *Genes Dev.* **21**, 2422–2432, (2007).

64. Y. Yang, *et al.*, Lymphatic endothelial progenitors bud from the cardinal vein and intersomitic vessels in mammalian embryos. *Blood* **120**, 2340–2348, (2012).

65. T. Mäkinen, *et al.*, Inhibition of lymphangiogenesis with resulting lymphedema in transgenic mice expressing soluble VEGF receptor-3. *Nat. Med.* **7**, 199–205, (2001).

66. M. Baker, *et al.*, Use of the mouse aortic ring assay to study angiogenesis. *Nat. Protoc.* **7**, 89–104, (2012).

67. A. W. B. Stanton, S. Modi, R. H. Mellor, J. R. Levick, P. S. Mortimer, Recent Advances in Breast Cancer-Related Lymphedema of the Arm: Lymphatic Pump Failure and Predisposing Factors. *Lymphat Res Biol* **7**, 29–45, (2009).

68. M. J. Weiler, M. T. Cribb, Z. Nepiyushchikh, T. S. Nelson, J. B. Dixon, A novel mouse tail lymphedema model for observing lymphatic pump failure during lymphedema development. *Sci. Rep.* **9**, 10405, (2019).

69. F. Pastouret, *et al.*, Anatomical Effects of Axillary Nodes Dissection on Rat Lymphatic System Model: Indocyanine Green Mapping and Dissection. *Lymphat Res Biol* **14**, 134–141, (2016).

70. T. S. Nelson, *et al.*, Lymphatic remodelling in response to lymphatic injury in the hind limbs of sheep. *Nat Biomed Eng*, 1–13, (2019), https:/doi.org/10.1038/s41551-019-0493-1.

71. S. Culemann, *et al.*, Stunning of neutrophils accounts for the anti-inflammatory effects of clodronate liposomes. *J. Exp. Med.* **220**, e20220525, (2023).

72. M. Peiseler, P. Kubes, More friend than foe: the emerging role of neutrophils in tissue repair. *J. Clin. Investig.* **129**, 2629–2639, (2019).

73. E. Güç, *et al.*, Local induction of lymphangiogenesis with engineered fibrin-binding VEGF-C promotes wound healing by increasing immune cell trafficking and matrix remodeling. *Biomaterials* **131**, 160–175, (2017).

74. Z. Hajjarian, *et al.*, Laser Speckle Rheology for evaluating the viscoelastic properties of hydrogel scaffolds. *Sci Rep-uk* **6**, 37949, (2016).

75. M. A. Kotlarchyk, *et al.*, Concentration Independent Modulation of Local Micromechanics in a Fibrin Gel. *Plos One* **6**, e20201, (2011).

76. E. M. Bouta, *et al.*, Lymphatic function measurements influenced by contrast agent volume and body position. *Jci Insight* **3**, e96591, (2018).

77. D. Allen, *Danny Allen (2022). Protein Array Tool (https://www.mathworks.com/matlabcentral/fileexchange/35128-protein-array-tool), MATLAB Central File Exchange. Retrieved October 12, 2022.*

78. E. Zudaire, L. Gambardella, C. Kurcz, S. Vermeren, A Computational Tool for Quantitative Analysis of Vascular Networks. *Plos One* **6**, e27385, (2011).

79. A. Torres-Espín, D. Santos, F. González-Pérez, J. del Valle, X. Navarro, Neurite-J: An Image-J plug-in for axonal growth analysis in organotypic cultures. *J Neurosci Meth* **236**, 26–39, (2014).

80. A. Lunde, J. C. Glover, A versatile toolbox for semi-automatic cell-by-cell object-based colocalization analysis. *Sci Rep-uk* **10**, 19027, (2020).

Funding:

National Institute of Health (NIH) F32HL156654 (MSR)
National Institute of Health (NIH) R01CA284603 (LLM,TPP)
National Institute of Health (NIH) R01CA284372 (TPP)
National Institute of Health (NIH) R21AG072205 (TPP)
National Institute of Health (NIH) R01HL128168 (LLM ,TPP)
National Institute of Health (NIH) R21EB031982 (LLM)
National Institute of Health (NIH) R01CA247441 (LLM)
Rullo Family MGH Research Scholar Award from the MGH Research Institute (TPP)

Author contributions:

Conceptualization: MSR, ZA, TPP, LLM
Methodology MSR, ZA, PL, NL, SN,KR,MO
Investigation: MSR, ZA, PL
Visualization: MSR, ZA
Supervision: TPP, LLM
Writing—– original draft: MSR, TPP, LLM– review & editing: All authors.

Competing interests: LLM has equity in Bayer AG and is a consultant for SymBiosis. Other authors declare they have no competing interests.

Data and materials availability: All data generated by this study are available within the Article, Supplementary Information, or available from the authors upon request (submit requests to lmunn@mgh.harvard.edu, mrazavi2@unl.edu or tpadera@mgh.harvard.edu).

Figures

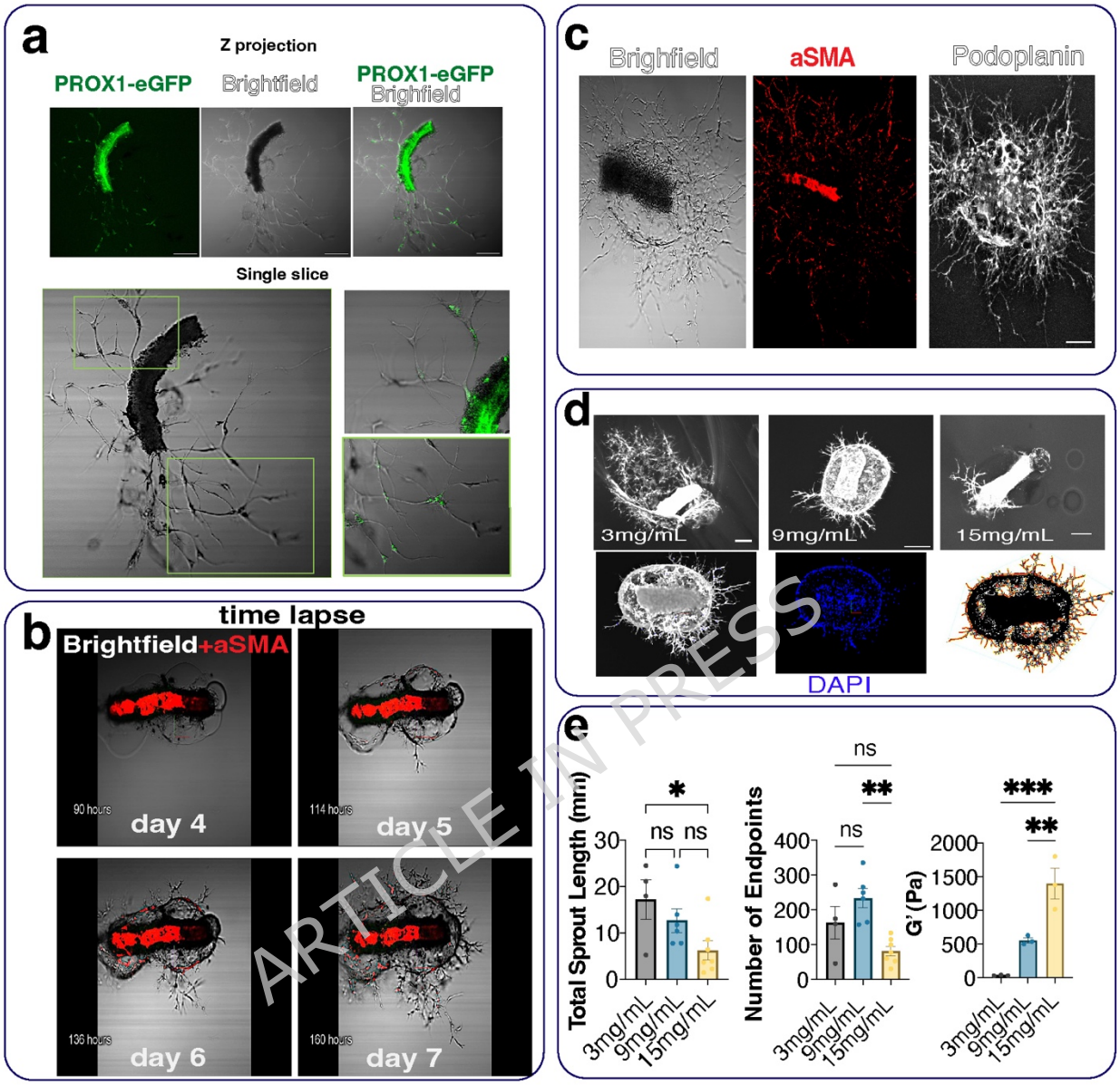

Figure 1. Fibrin gel supports lymphatic sprouting *in vitro*, and the sprouting response varies with fibrinogen concentration. a) Representative image of a segment of a collecting lymphatic vessel isolated from a PROX1eGFP mouse reporter embedded in fibrin gel for 9 days. Phase-contrast imaging shows the vessel explant and sprouts in the fibrin gel; PROX1-eGFP indicates LECs **b)** Representative time-lapse imaging illustrates the time course of sprout formation, LMC migration (DsRed- αSMA+ cells), and fibrin gel degradation. **c)** A representative image of lymphatic sprouts shows that vessels and sprouts are positive for Podoplanin (Alexa-647, white) and LMC (αSMA (Cy3, red)), indicating lymphatic endothelial and muscle cells, respectively. **d)** Representative images of sprouts stained with lectin (DyLight™ 649) at different fibrinogen concentrations demonstrate how sprouting varies as fibrinogen concentration increases (3 mg/mL, 9 mg/mL, and 15 mg/mL). Also presented (lower panels) is a 3D reconstruction of sprouts at a concentration of 9 mg/mL with DAPI staining, including a z-projection image, image segmentation, and sprout quantification. **e)** Sprouting metrics (total length of sprouts and total number of endpoints) were quantitatively analyzed with AngioTool software. Quantification of the elastic properties of fibrin gel at different concentrations reveals that the elastic storage modulus (G') increases significantly with increasing fibrinogen concentration. One-way ANOVA analysis with a Tukey post hoc test was used to determine statistical significance between groups (*$p < 0.05$, **$p < 0.01$, ***$p < 0.001$). The scale bar represents 200 µm. All data are presented as mean (± SEM).

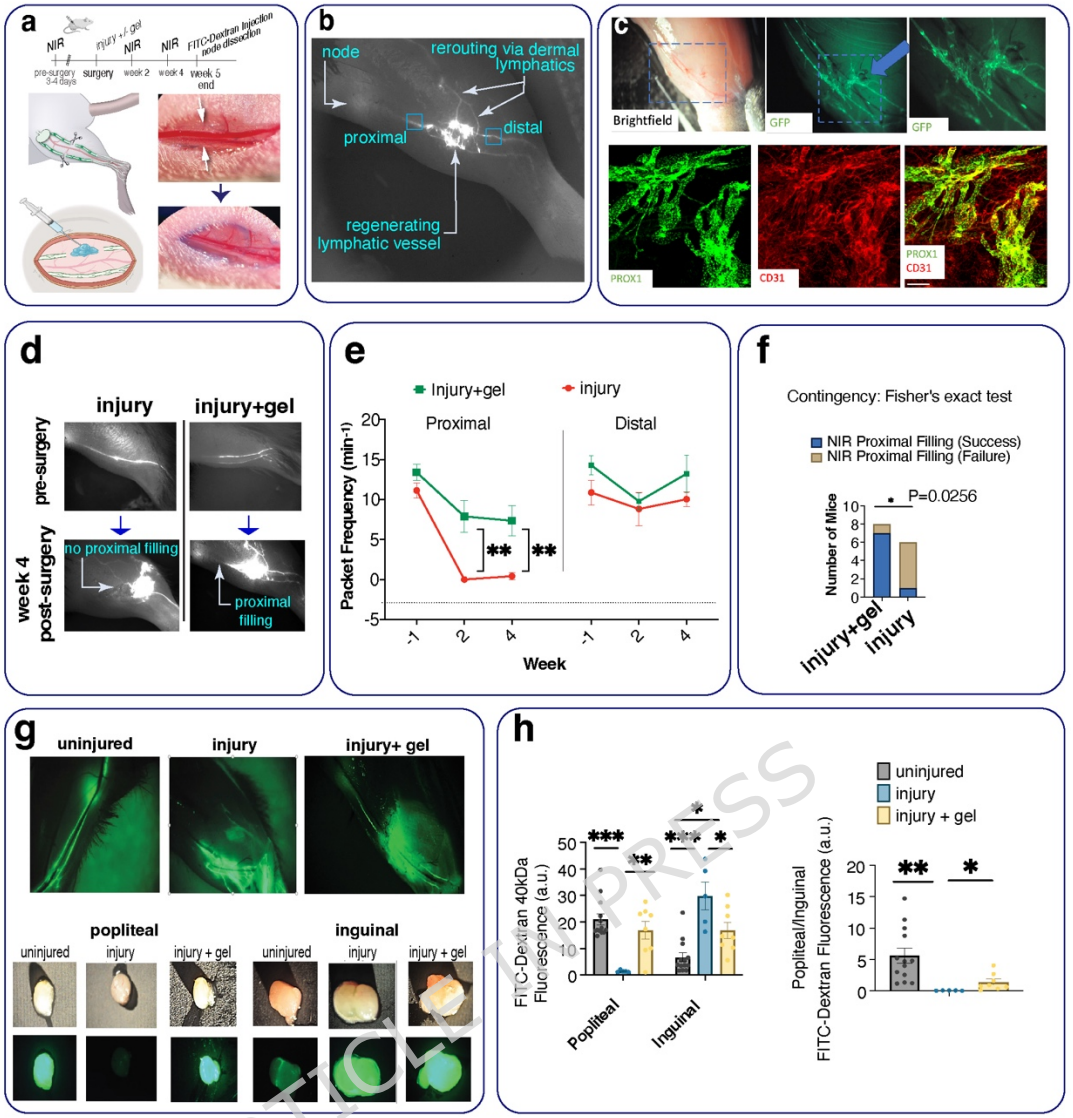

Figure 2. Fibrin gel implantation promotes lymphatic regeneration and restoration of lymphatic transport to the draining lymph node after lymphatic vessel ligation. a) Schematic representation of lymphatic surgery where both saphenous lymphatic vessels were surgically ligated, and fibrin gel was implanted. **b)** A representative NIR imaging of mouse hindlimb at four weeks after gel implantation showing reconnection of injured lymphatic vessels as well as rerouting of lymphatic flow to the dermal lymphatic vessels. **c)** Representative confocal imaging showing lymphatic sprouts form from injured collecting vessels following gel implantation to reconnect injured vessel. The image was taken 3 weeks post-injury, where PROX1eGFP+ cells indicate LECs and CD31 shows BECs. The scale bar indicates 200µm. **d)** Representative longitudinal imaging of lymphatic pumping was captured by a near-infrared imaging (NIR) system, showing popliteal collecting lymphatic vessels before lymphatic surgery and two weeks after injury with and without fibrin gel implantation. **e)** Functional NIR imaging was used to evaluate the restoration of lymphatic pumping in mice that had undergone collecting vessel injury with or without gel implantation (n=6 for injury, n=8 for injury plus gel). Packet frequency, or the number of packet pulsations, was quantified at locations distal and proximal to the site of lymphatic injury. **f)** At 4 weeks post-injury, mice with gel implantation are more likely than mice without gel implantation to have the filling of collecting lymphatic vessels proximal to the injury restored (two-sided Fisher' exact test $p<0.05$) **g)** Representative images show the uptake of 40kDa-FITC into the popliteal and inguinal lymph nodes following lymphatic injury, with or without gel implantation five weeks post-injury, measured 3 hours after injection. **h)** Quantification of 40kDa-FITC accumulation in the popliteal and inguinal lymph nodes after lymphatic injury with and without gel implantation shows the lymph uptake to the popliteal draining node is restored following gel implantation. After injecting 10 µl of 40 kDa-FITC dye into the paw, the lymph nodes were harvested after 3 hours. The harvested lymph nodes were then homogenized in PBS, and their fluorescence was measured using a fluorometer. Lymph nodes from both the injured legs (with or without gel) and the uninjured legs (control) of mice were analyzed. Unpaired t-test was used to test for significant differences between the NIR metrics of the injured and gel implantation groups at each time (*$p < 0.05$, **$p < 0.01$). ANOVA with Tukey post hoc test was used to test the significant difference in FITC uptake (*$p < 0.05$, **$p < 0.01$, **$p < 0.001$). All data were presented as mean (±s.e.m.).

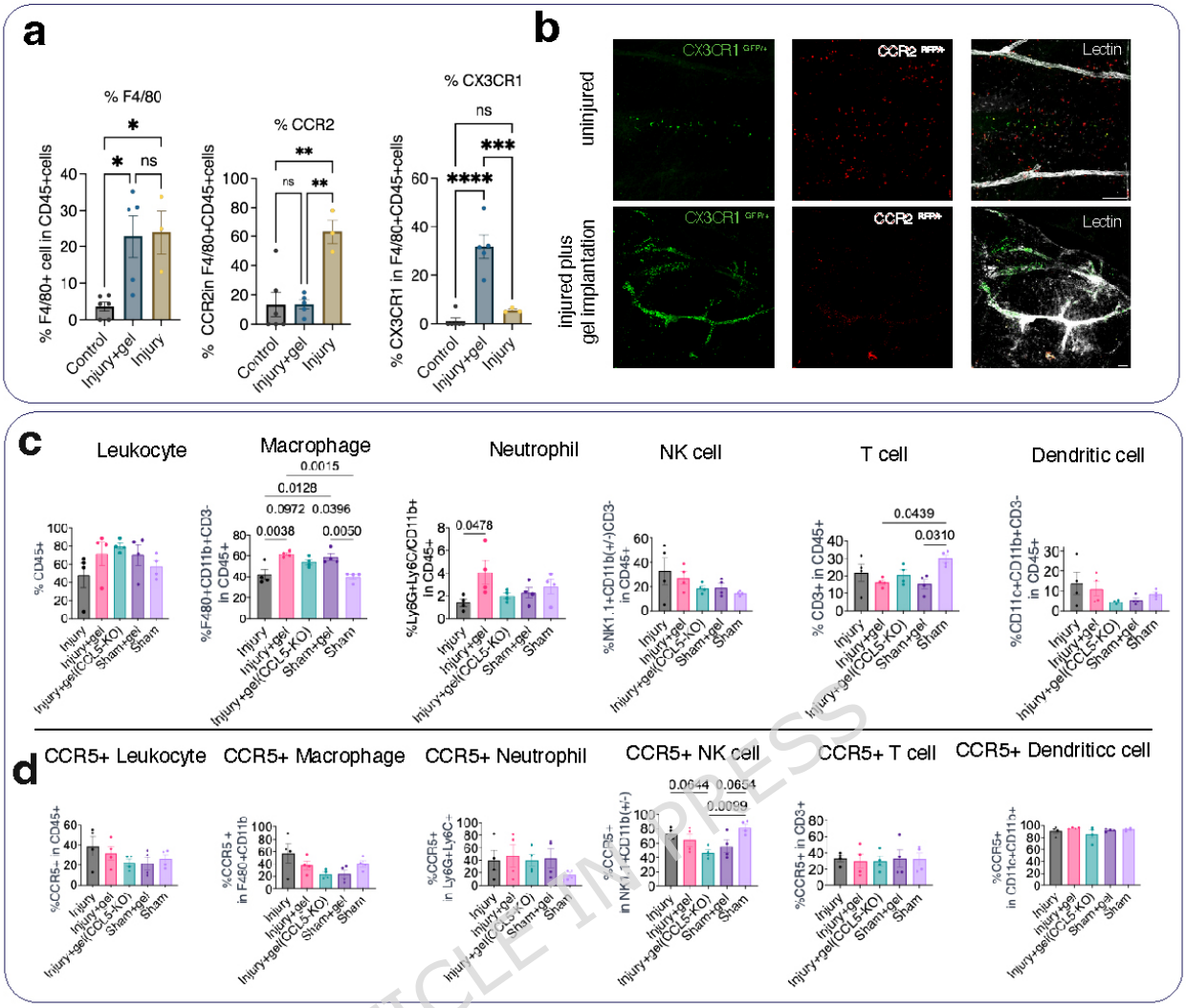

Figure 3. Fibrin gel implantation following lymphatic injury results in macrophage and neutrophil recruitment. a) Percentage of macrophage infiltration on day 10 after lymphatic injury in the absence and presence of fibrin gel measured by flow cytometry. **b)** Representative confocal images of the tissue surrounding uninjured and injured collecting lymphatic vessels with gel implantation. The data show that two weeks post-gel implantation, CX3CR1(+) and CCR2(+) cells accumulate around the regenerating vessel, where lectin-647 (white) indicates saphenous lymphatic vessels (see also Supplementary Figure S6**). c-d)** The top panel illustrates the percentage of various cell types within the CD45+ population. The bottom panel shows the percentage of CCR5+ cells within each identified population. Each group comprised 4 mice, with tissue dissection and flow cytometry conducted 10 days following injury and gel implantation. ANOVA and post-hoc Tukey HSD tests were utilized to determine statistical significance. P-values are presented for statistically significant groups.

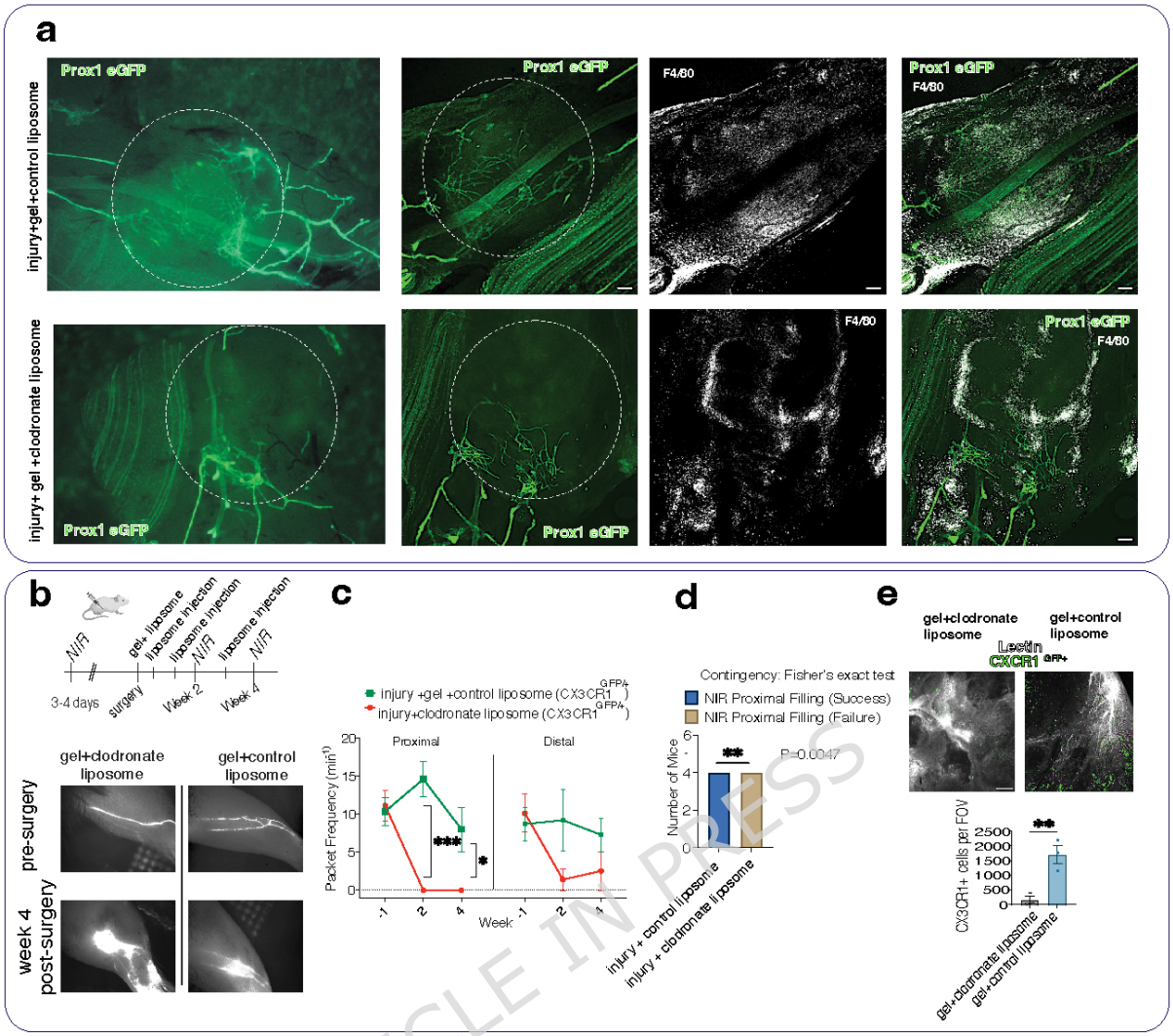

Figure 4: Macrophage and neutrophil depletion abolishes lymphatic regeneration after fibrin gel implantation. a) Representative epifluorescence and confocal images of mouse saphenous tissue treated with control and clodronate liposomes after injury showing clodronate liposomes abolished lymphatic endothelial sprouting (PROX1-GFP+) within the fibrin gel. Mice treated with control liposomes exhibit lymphatic sprouting and reconnection within the gel. The fibrin gel was loaded with 10% v/v clodronate or control liposomes prior to polymerization in vivo. The white circle indicates the approximate injury site, and the white arrows show the direction of lymphatic flow. **b)** Longitudinal near-infrared imaging was used to assess lymphatic pumping and regeneration after macrophage depletion by clodronate liposomes (n = 4) and control liposomes (n = 4) using CX3CR1GFP/+ mice. Representative NIR images of the popliteal collecting lymphatic vessels before surgery, two and four weeks after fibrin gel implantation. The red and blue arrows indicate lymphatics distal and proximal to the injury site, respectively. **c)** Analysis of functional NIR imaging reveals a lack of lymphatic regeneration and loss of lymphatic pumping (packet frequency) after treatment by clodronate liposomes proximal to the injury site. **d)** After gel implantation and treatment with clodronate liposomes in CX3CR1 GFP/+ mice, injured collecting lymphatic vessels did not adequately regenerate to re-connect the injured vessels (failure of proximal filling). In contrast, CX3CR1 GFP/+ mice treated with control liposomes successfully reconnected injured vessels (success of proximal filling two-sided Fisher's Exact test $p<0.05$). **e)** Confocal imaging was used to evaluate the depletion success in CX3CR1$^{GFP/+}$ mice. Quantification of CX3CR1+ cells shows that the number of cells significantly decreased following treatment by clodronate liposomes (n=3). Statistically significant differences between presurgical values and values on days 14, and 28 following injury were tested via ANOVA with Tukey's post hoc tests (*$p < 0.05$, **$p < 0.01$). An unpaired t-test was used to test for significant differences between the control liposomes and clodronate liposome groups at each time (*$p < 0.05$, ** $p<0.01$).

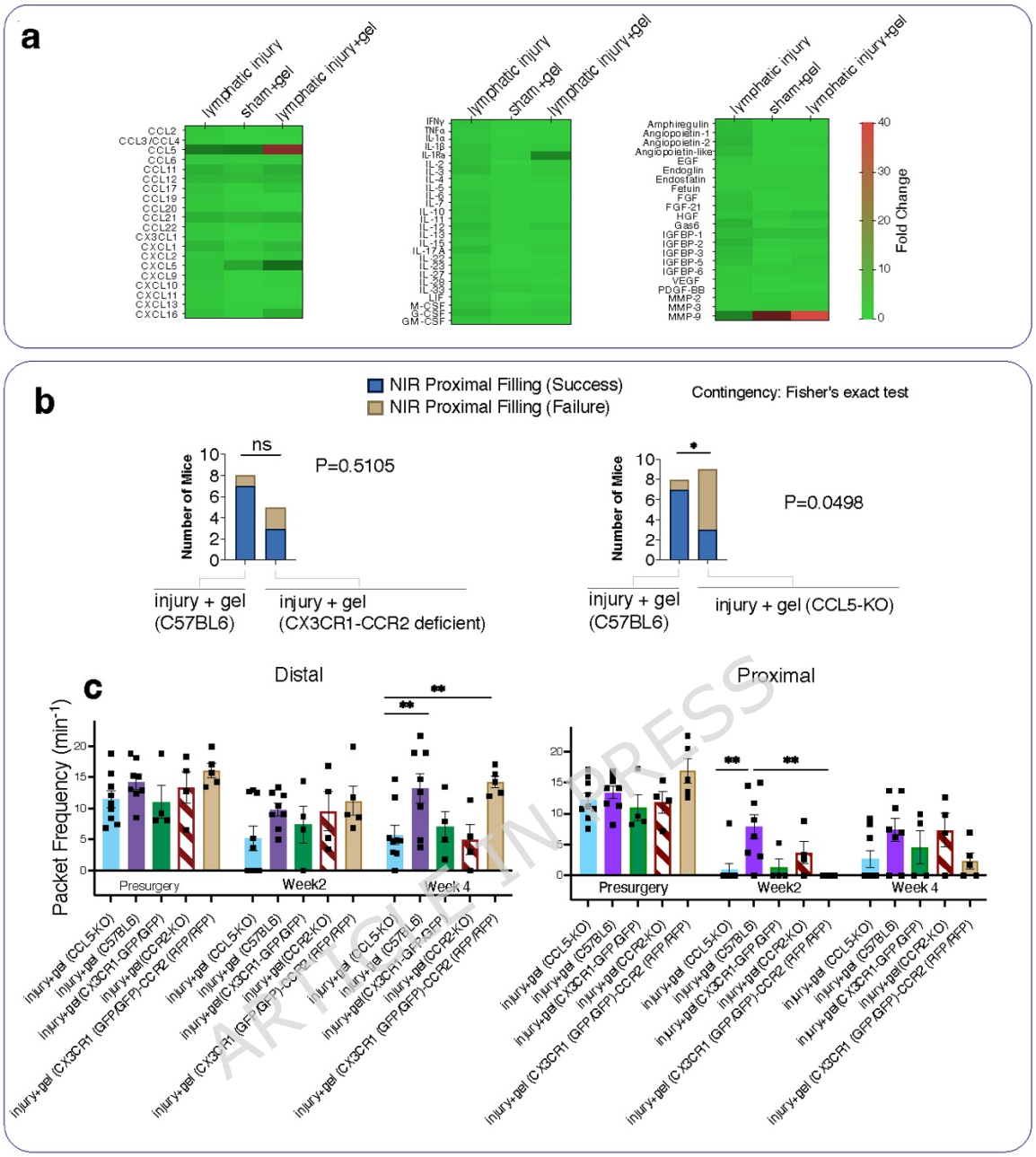

Figure 5. Fibrin gel implantation leads to increased tissue CCL5 after lymphatic vessel injury and loss of CCL5 inhibits the recovery of lymphatic filling proximal to the injury site. a) A comparative analysis of the levels of cytokines and growth factors after gel implantation demonstrating the upregulation of CCL5 and MMP9 (n=3 mice pooled in each group). Data generated by Proteome Profiler Cytokine Array (R&D systems, Minneapolis, MN) according to the manufacturer's protocol. The values indicate fold changes in different groups relative to the values in the sham group. b) Mice lacking CCL5 (CCL5-/-) cytokine are less likely than control mice to regain filling of vessels proximal to the injury site (proximal filling) subsequent to gel implantation 4-week post-injury (p=0.0498, two-sided Fisher's Exact Test) while deficiency of CX3CR1 and CCR2 are not associated with the success/failure of proximal filling recovery following gel implantation (p=0.5105, two-sided Fisher's Exact Test). **c)** A comparison of lymphatic pumping frequencies via NIR technique proximal and distal to the injury site among CCL5-KO, CX3CR1(GFP/GFP), CCR2(-/-), and double-deficient CX3CR1(GFP/GFP)-CCR2(RFP/RFP) mice following gel implantation. To test the association between categorical variables (success/ failure of proximal filling after gel implantation), the two-sided Fisher's Exact test was used ($p < 0.05$). One-way ANOVA analysis with the Tukey post hoc test was used to test the significant difference between different groups after gel implantation (*$p < 0.05$, **$p < 0.01$, ***$p < 0.001$). All data were presented as mean (±s.e.m.).